Analysis of Carrier Overlap Modulation and Space Vector Modulation Equivalence in NPC Inverters

Haoting Du, *Student Member, IEEE*, Yingjie He, *Senior Member, IEEE*, Zhengchen Zhao, Shenglun Zhuang, and Jinjun Liu, *Fellow, IEEE*

***Abstract*—Carrier overlapping pulsewidth modulation (COPWM) is proposed to address the level degradation issue in carrier-based pulsewidth modulation (CBPWM) at low modulation index. Due to its unique frequency multiplication band, COPWM has widespread application in industrial scenarios where long-term operation at low modulation index is required. Similarly, space vector pulsewidth modulation (SVPWM) exhibits more switching states at low modulation index, and the output performance can be enhanced by increasing the number of modulation segments. Numerous literature studies have analyzed the equivalence relationship between CBPWM and SVPWM methods. However, there is no research on the equivalence relationship between COPWM and SVPWM methods. Investigating the relationship between the two methods is beneficial for us to draw upon the strengths of both modulation techniques and develop more effective modulation methods. This article analyzes the relationship between COPWM and SVPWM methods under different modulation index and overlap ratios. It is concluded that as the modulation index and overlap ratio increase, the synthesis method of the reference vector in the equivalent SVPWM method for the COPWM method tends to become irregular. Subsequently, by adjusting the active time of redundant states of space vectors, the SVPWM method achieves output equivalence to the COPWM method. Finally, experimental results confirm the correctness and effectiveness of the proposed approach.**

***Index Terms*—Carrier overlapping pulsewidth modulation (COPWM), equivalence relationship, five-Level NPC-inverter, space vector pulsewidth modulation (SVPWM).**

I. Introduction

CARRIER-BASED pulsewidth modulation (CBPWM) is the most widely used modulation strategy in multilevel inverters due to its simplicity and ease of implementation. However, as the number of voltage levels increases, CBPWM suffers from level degradation at low modulation index [1], [2], [3], [4], [5]. Switching devices are not fully utilized in this case. To address this issue, the carrier overlapping PWM (COPWM) method is proposed. COPWM shares the same advantages as CBPWM in terms of simplicity and ease of implementation for high-level inverters. Additionally, COPWM is suitable for industrial scenarios that require long operation at low modulation index, profit from its unique frequency multiplication band and the freedom to utilize both vertical and horizontal dimensions. In [6], a hybrid COPWM approach is applied to improve waveform quality at low modulation index in cascaded H-bridge inverters. In [7], a novel COPWM method specifically designed for flying capacitor inverters is proposed, which enhances waveform quality at low modulation index for such inverter configuration. [8] introduced an innovative COPWM technique enabling the accurate realization of NP potential control in a four-level neutral point clamped (NPC) inverter. This new method can achieve the natural voltage balance of three dc-link capacitors under ideal and steady states. A COPWM method tailored for NPC multilevel converters was proposed in [9], facilitating the effective balancing of dc voltages in these inverters. With this modulation method, the average values of all the neutral-point currents are equal to zero in a fundamental period, and therefore, all the dc-link capacitor voltages can be naturally balanced in the ideal and steady-state conditions. Wang et al. [10] delved into a focused examination of five-level NPC inverters and presented a modulation technique designed to achieve NP potential balance within these inverters. The concept of addressing dc-side capacitors' voltage balance through an approach of outer-to-inner progression. The top and the bottom dc-link capacitor voltages are balanced by zero-sequence voltage injection. The two inner capacitor voltages are balanced by adjusting the width of switching signals. A novel composite modulation technique was introduced in [11]. For a low modulation index range under 0.5, phase disposition pulsewidth modulation is utilized and a zero-sequence voltage injection-based NP voltage balancing method was proposed in this method. For a high modulation index range more than 0.5, a decoupled voltage-balancing method based on COPWM is used. By combining the two modulations and voltage-balancing methods, the NP voltages can be balanced under the full modulation index range with reduced switching losses. In [12], a new four-level ANPC inverter topology is introduced along with a unique COPWM technique tailored to

Received 18 August 2024; revised 27 November 2024; accepted 31 December 2024. Date of publication 8 January 2025; date of current version 26 February 2025. This work was supported in part by the "Qinchuangyuan Scientist + Engineer" Program of Shaanxi Province under Grant 2024QCY-KXJ-138, in part by the Aeronautical Science Foundation of China under Grant 20230040070017, in part by the National Natural Science Foundation of China under Grant 51777158, and in part by the "Chunhui Plan" Cooperative Research Project of the Education Ministry under Grant 202200765. Recommended for publication by Associate Editor B. Mirafzal. *(Corresponding author: Yingjie He.)*

Haoting Du, Yingjie He, and Zhengchen Zhao are with the Department of Industrial Automation, School of Electrical Engineering, Xi'an Jiaotong University, Xi'an 710049, China (e-mail: tommydht@stu.xjtu.edu.cn; yjhe@mail.xjtu.edu.cn; zczhao@stu.xjtu.edu.cn).

Shenglun Zhuang is with NARI Group Corporation, Nanjing 211000, China (e-mail: zhuangshenglun@sgepri.sgcc.com.cn).

Jinjun Liu is with the School of Electrical Engineering, Xi'an Jiaotong University, Xi'an 710049, China (e-mail: jjliu@mail.xjtu.edu.cn).

Color versions of one or more figures in this article are available at https://doi.org/10.1109/TPEL.2025.3526767.

Digital Object Identifier 10.1109/TPEL.2025.3526767

achieve NP potential balance. The upper and lower dc-link capacitor voltages are balanced by zero-sequence voltage injection and the central dc-link capacitor voltage is balanced by adjusting the duty cycles of switching signals slightly.

The SVPWM method exhibits superior modulation performance, but it suffers from disadvantages such as complex calculations, difficult programming, and limited scalability. It is commonly applied in inverters with no more than five voltage levels [13], [14], [15], [16], [17]. Similarly, SVPWM possesses more switching states at low modulation index, and the output can be improved by increasing the number of modulation segments [18], [19], [20]. [21], [22], [23], [24], [25] compares the output voltage waveform quality of SVPWM and CBPWM methods at different modulation index. The study reveals that the SVPWM method achieves significantly lower total harmonic distortion in the output voltage waveform at low modulation index compared to the CBPWM method.

Based on the similar application scenarios and comparable effects mentioned above, it can be inferred that there exists a certain equivalence between COPWM and SVPWM methods. However, the current research on equivalence mainly focuses on the relationship between CBPWM and SVPWM methods [26], [27], [28], and there is a lack of investigation into the equivalence relationship between COPWM and SVPWM methods. Exploring the relationship between the two methods is beneficial for leveraging their advantages and developing superior modulation techniques.

This article focuses on the widely used five level-NPC inverter in industrial applications and analyzes the inherent connection between COPWM and SVPWM methods. The study investigates the influence and characteristics of different overlap ratios on the equivalent SVPWM method's vector sequence. Subsequently, the SVPWM method is used to achieve the same output performance as the COPWM method. Finally, experimental verification of the proposed equivalent method is conducted.

The contributions of this article are given as follows.

1) Investigates the fundamental principles of the COPWM method and SVPWM method for a five-level diode clamped inverter.
2) The output sequences of the COPWM method under different overlap ratios were analyzed, leading to the identification of a corresponding method for synthesizing equivalent space vectors. The impact of the overlap ratio and modulation index on the synthesis of equivalent space vectors was also analyzed.
3) Proposing an implementation approach to achieve the equivalent output performance of the COPWM method using the SVPWM method. Experimental verification is conducted to validate the correctness and effectiveness of this approach.

II. Carrier-Overlapping PWM Method

COPWM is a novel PWM method based on two degrees of freedom, the displacement in the vertical direction and the horizontal displacement between the carriers of a multilevel converter.

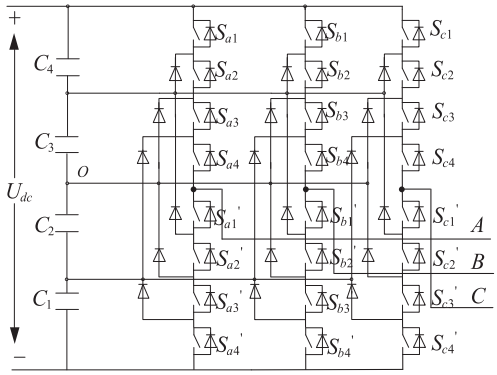

Fig. 1. Nonisolated five-level NPC inverter topology.

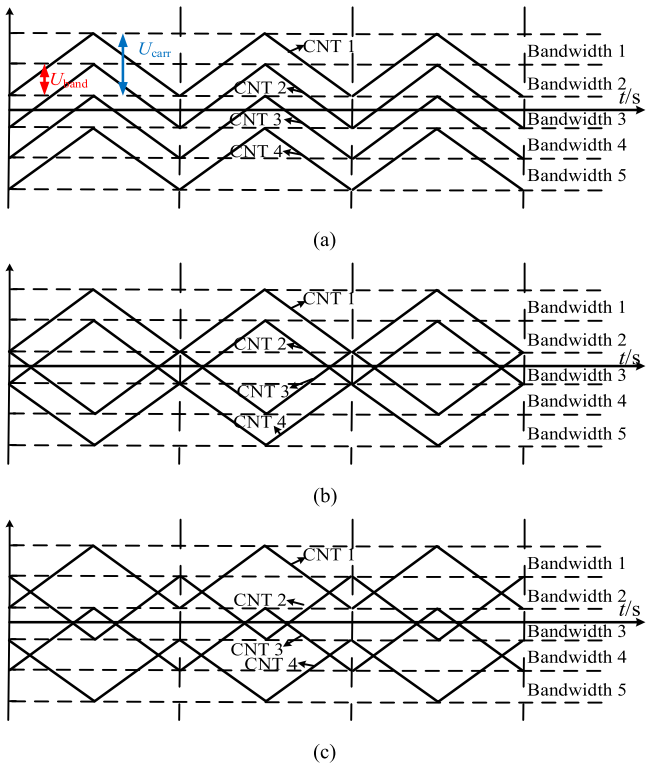

Fig. 2. Schematic of the five-level COPWM method. (a) 5-Level Same Direction Carrier Overlapping Strategy (COPWM-A). (b) 5-Level Opposite Direction Carrier Overlapping Strategy (COPWM-B). (c) 5-Level Same and Opposite Direction Carrier Overlapping Strategy (COPWM-C).

For the five-level NPC inverter topology shown in Fig. 1, COPWM methods are currently classified into three main categories, and their modulation waveforms are shown in Fig. 2. From [13] it can be known that the line voltage output from the COPWM-A modulation method is the best among the three methods, both in terms of harmonic spectrum and harmonic content. COPWM-B is the second best and COPWM-C is the worst. In this article, COPWM-A, which has the best modulation effect, is chosen as an example to be analyzed and discussed.

As shown in Fig. 2(a), two neighboring carriers are overlapped in carrier bands 2–4. COPWM operates on the same principle as CBPWM, where carriers 1–4 are compared with the modulating

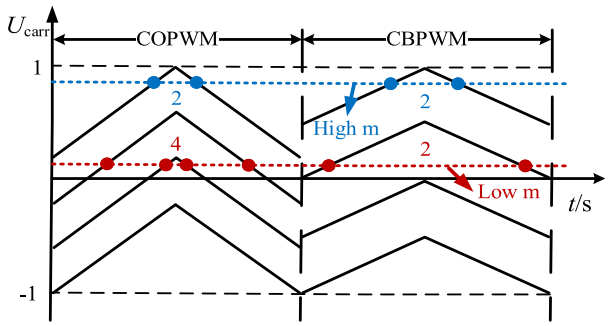

Fig. 3. Compare of the five-level COPWM and CBPWM.

TABLE I
FIVE LEVEL-NPC INVERTER SWITCHING STATUS

Output Voltage	On-off state of each Switch								State
	S_{i1}	S_{i2}	S_{i3}	S_{i4}	S_{i1}'	S_{i2}'	S_{i3}'	S_{i4}'	S_i
$U_{dc}/2$	1	1	1	1	0	0	0	0	4
$U_{dc}/4$	0	1	1	1	1	0	0	0	3
0	0	0	1	1	1	1	0	0	2
$-U_{dc}/4$	0	0	0	1	1	1	1	0	1
$-U_{dc}/2$	0	0	0	0	1	1	1	1	0

note: i=a,b,c

waveforms to give the switching states of switching tubes 1–4 directly. Define the overlap ratio C as the ratio of the height of the interleaved band to the height of the carrier

$$C = \frac{U_{\text{band}}}{U_{\text{carr}}} \times 100\%. \tag{1}$$

Among it, U_{band} is the height of the overlap band and U_{carr} is the amplitude of the carrier as shown in Fig. 2(a).

As can be seen from the points of intersection of the modulating waveform and the carrier in Fig. 3, the COPWM method differs from the CBPWM method in that the COPWM method, because of the existence of the overlapped bands, at lower modulation index, the modulating waveform intersects with more than one carrier in a switching cycle, generating multiple points of intersection, while the CBPWM method will only intersect with one carrier, generating two points of intersection. At higher modulation index, the COPWM method is the same as the CBPWM method in that the modulating waveform will intersect only one carrier in a switching cycle, producing two intersections. Thus, for the COPWM method, because of the presence of carrier overlapping bands, the switching utilization can be optimized, the switching frequency can be increased, the output waveform quality can be improved in a low modulation index, and good harmonic performance can be achieved.

III. SPACE VECTOR PWM METHOD

According to the five-level NPC inverter topology in Fig. 1, the five-level states are defined as 01,23, and 4. Taking phase I (I = A, B, C) as an example, there are eight switching tubes in this phase, denoted as S_{i1}, S_{i2}, S_{i3}, S_{i4}, S'_{i1}, S'_{i2}, S'_{i3}, and S'_{i4}. The switching states of S_{ij} and S'_{ij} $(j = 12, 34)$ are always reversed. When S_{ij} is all turned on, this state is defined as $S_i = 4$. Other states are given in Table I.

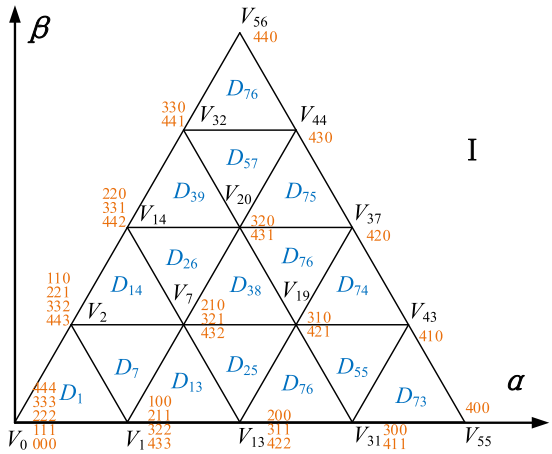

Fig. 4. Sector I space vector diagram for five-level inverter.

The five-level space vector diagram is shown in Fig. 4, defining the modulation index of the five-level inverter as

$$m = \frac{3\,|V_{\text{ref}}|}{2U_{\text{dc}}} \tag{2}$$

$|V_{\text{ref}}|$ is the magnitude of the reference voltage vector V_{ref}, and $2U_{\text{dc}}/3$ is the magnitude of the large vector.

As shown in Fig. 4, the space vector diagram can be divided into six large triangular regions, respectively, for the I, II, III, IV, V, and VI sectors. Each large sector contains 16 small triangles, the first large sector (0°–60°) as an example of a simple introduction to the synthesis process of the reference vector.

When the reference vector is located in the D_1 region shown in Fig. 4, the synthesis process of the reference vector is synthesized by the zero vector V_0 and two small vectors V_1 and V_2 according to

$$\begin{cases} V_{\text{ref}} = V_0 \times T_0 + V_1 \times T_1 + V_2 \times T_2 \\ T_0 + T_1 + T_2 = T_S \end{cases} \tag{3}$$

where V_{ref} is the reference vector and T_0, T_1 and T_2 are the durations of the vectors V_0, V_1, and V_2, in one switching cycle T_{s}.

The previous analysis shows that the switching sequence of the vector modulation output is not unique because some of the voltage vectors in the five-level space vector diagram contain redundant switching states. When the reference vector V_{ref} of the five-level inverter is in sector D_1, V_{ref} is synthesized from three voltage vectors, V_0, V_1 and V_2, V_0 is a zero vector, which contains five redundant switching states, V_1 and V_2 are both small vectors, and both contain 4 redundant switching states. Switching combinations generally begin and end with a zero vector. In sector D_1, there are a total of 3 vectors and 13 switching states, and by utilizing all the switching states, the longest output vector switching combination can be obtained, which can be expressed as: (000) = > (100) = > (110) = > (111) = > (211) = > (221) = > (222) = > … = > (443) = > (444). The length of the corresponding SVPWM sequence is 26 segments, and this sequence is called the all-switching sequence.

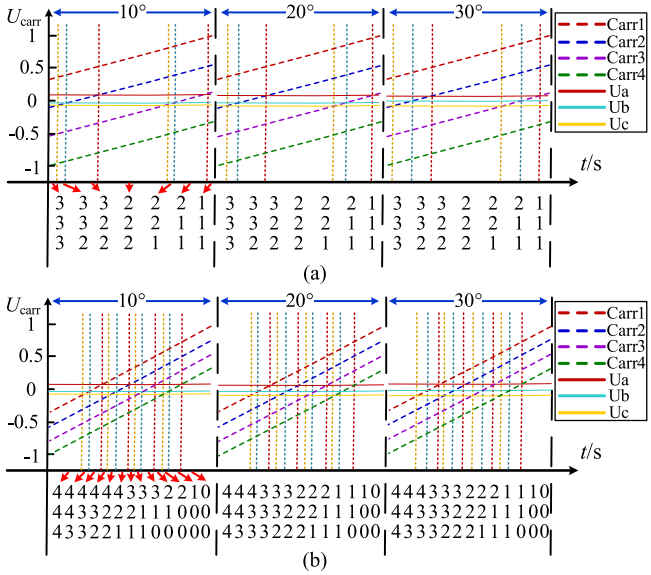

Fig. 5. Illustration of reference vector synthesis when m = 0.1. (a) C = 33.3%. (b) C = 83.3%.

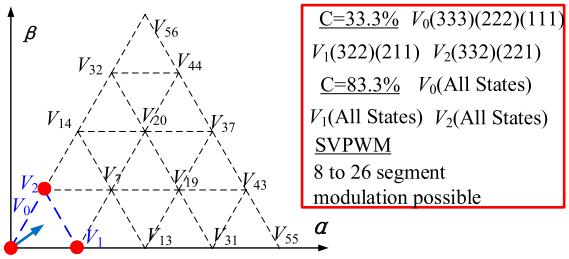

Fig. 6. Spatial vector partition of the reference vector rotating to 20° for the conventional SVPWM method, as well as the COPWM method with $C = 33.3\%$ and $C = 83.3\%$ when $m = 0.1$.

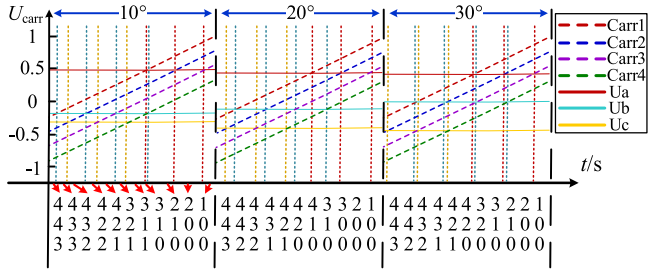

Fig. 7. Synthesis of the reference vector for $C = 83.3\%$, $m = 0.5$.

In actual applications, a sequence of switch combinations can be obtained between 8 to 26 segments arbitrarily by selecting only four or more of these switch states to synthesize the reference vector according to the modulation requirements.

IV. Equivalent Analysis of the SVPWM Method and COPWM Method

A. Division of Space Sectors for New Modulation Strategy and the Basic Principle of Leakage Current Suppression

Analysis of the reference vector synthesis method for the five-level COPWM method is discussed for the case where the reference vector is rotated within the first large sector with $C = 83.3\%(33.3\%)$ and the modulation index is taken as 0.1, 0.3, and 0.5. Because the synthesis rule of the vectors is axisymmetric about the center line (30° line) of the sector I, that is to say, although the vectors used when the reference vectors are rotated to 10° and 50° may be different, they have the same synthesis rule for the reference vectors. Therefore, the analysis of the reference vector synthesis rule in this section looks at the process of rotating the reference vector from 0° to 30°.

1) The relationship between the reference vector synthesis methods of COPWM and SVPWM Methods.

When $m = 0.1$, the synthesis of the reference vectors at different operating angles is shown in Fig. 5.

From Fig. 5, it can be observed that when $C = 33.3\%$, the modulation wave intersects with two carrier waves. The modulation sequence for half a cycle is (333) = > (332) = > (322) = > (222) = > (221) = > (211) = > (111).

By examining the modulation sequence, it is evident that this segment contains redundant states for V_0, V_1, and V_2, with a total of 14 modulation segments. When $C = 83.3\%$, the modulation wave intersects with four carrier waves. The corresponding modulation sequence is (444) = > (443) = > (433) = > (333) = > (332) = > (322) = > (222) = > ... = > (100) = > (000). From the modulation sequence, it can be observed that this segment contains all the redundant states for V_0, V_1 and V_2. In this case, the modulation consists of a total of 26 segments, forming a complete modulation sequence.

By comparing the results, it can be observed that as the overlap ratio increases, the number of modulation segments increases, leading to an increase in the number of switching actions. However, the modulation effectiveness improves. From the modulation sequence, it can be seen that the modulation sequence of the COPWM method and the conventional SVPWM method are partitioned as shown in Fig. 6. Both methods utilize the three nearest vectors to synthesize the reference vector. The difference lies in the fact that the SVPWM method can achieve modulation with any number of segments, ranging from 8 to 26, while the number of modulation segments in COPWM is influenced by the overlap ratio.

When $m = 0.5$, the synthesis method of the reference vector in the COPWM(C = 33.3%) method is the same as the conventional SVPWM method, as depicted in Fig. 8(a).

However, a significant difference arises in the synthesis method of the reference vector between the COPWM($C = 83.3\%$) method and the conventional SVPWM method. The specific modulation sequence is illustrated in Fig. 7. From Fig. 7, it can be observed that when the reference vector rotates to 10°, it is located near sector D_{13} in Fig. 3. The COPWM($C = 83.3\%$) method utilizes eight different vectors for modulation, as shown in Fig. 8(b). Under the same conditions, the conventional SVPWM method and the COPWM($C = 33.3\%$) method employ the nearest-three-vector modulation approach, as depicted in Fig. 8(a). However, the conventional SVPWM method allows for modulation spanning from 8 to 20 segments, while the

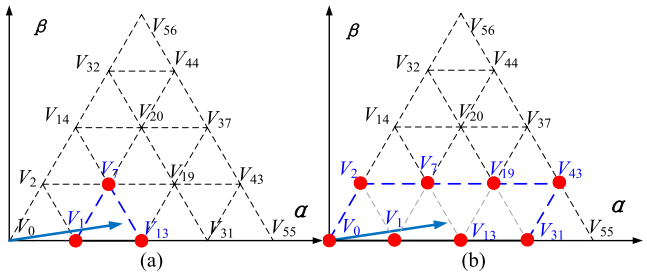

Fig. 8. Comparison of space vector synthesis methods for conventional SVPWM, COPWM($C = 33.3\%$) method and COPWM($C = 83.3\%$) method with reference vector rotated to 10° at $m = 0.5$. (a) Conventional SVM and C = 33.3%. (b) C = 83.3%.

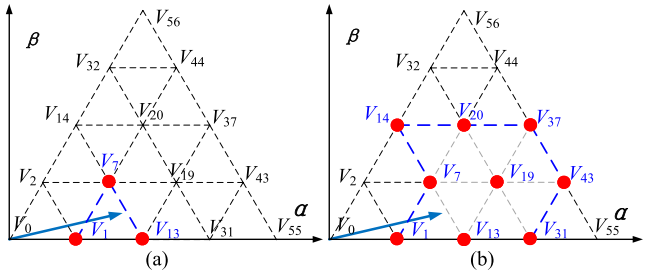

Fig. 9. Comparison of space vector synthesis methods for conventional SVPWM, COPWM($C = 33.3\%$) method and COPWM($C = 83.3\%$) method with reference vector rotated to 20° at $m = 0.5$. (a) Conventional SVM and C = 33.3%. (b) C = 83.3%.

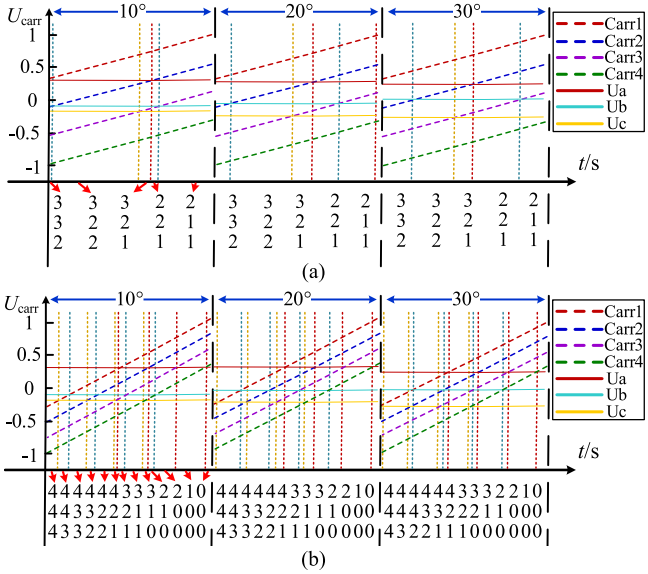

Fig. 10. Schematic of the synthesis of the reference vector at $m = 0.3$. (a) C = 33.3%. (b) C = 83.3%.

COPWM($C = 33.3\%$) method adopts a fixed ten segments modulation. In this modulation, two redundant states (322) and (211) of V_1, one redundant state (321) of V_7, and two redundant states (422) and (311) of V_{13} are utilized.

When the reference vector rotates to 20°, the modulation sequence employed by the COPWM($C = 83.3\%$) method utilizes the surrounding 10 vectors as illustrated in Fig. 9(b). Under the same conditions, the conventional SVPWM method and the COPWM($C = 33.3\%$) method adopt the nearest-three-vector modulation approach shown in Fig. 8(b). The conventional SVPWM method, similar to when the reference vector is at 10°, allows for modulation spanning from 8 to 20 segments.

In contrast, the COPWM($C = 33.3\%$) method increases the number of segments to 14 compared to 10°. In this modulation, two redundant states (322) and (211) of V_1, three redundant states (432), (321), and (210) of V_7, and two redundant states (422) and (311) of V_{13} are utilized.

By comparing Fig. 7(a) and (b) and Fig. 8(a) and (b), it is evident that due to the increase in overlap ratio, the reference vector synthesis method of the COPWM method transforms synthesizing the reference vector using the nearest three vectors, similar to the conventional SVPWM method. Instead, it now utilizes approximately ten to ten vectors in the vicinity of the reference vector for synthesis. This clearly demonstrates that an increase in overlap ratio affects the effective spatial vector synthesis method of the COPWM method. By comparing Fig. 6(b) and Fig. 9(b), it is evident that with the increase in modulation index, the reference vector synthesis method of the COPWM method differs from the reference vector synthesis method of the conventional SVPWM method. While the SVPWM method synthesizes the reference vector by considering the nearest three vectors, the COPWM method utilizes approximately ten vectors in the vicinity for reference vector synthesis. This illustrates that the increase in modulation index also affects the effective spatial vector synthesis method of the COPWM method. Therefore, the reference vector synthesis method of the equivalent SVPWM method for the COPWM method is influenced by both the modulation index and overlap ratio variables.

2) relationship between the output voltages of COPWM and SVPWM methods.

As shown in Fig. 10(a), the modulation sequence of the COPWM($C = 33.3\%$) method when $m = 0.3$ is depicted. The modulation sequence reveals that distinct patterns emerge when the reference vector is positioned around 10° and 30°.

The modulation sequence when the reference vector is at 10° is (333) => (332) => (322) => (222) => (221) => (211) => (111), and when it is at 30°, the modulation sequence is (333) => (332) => (322) => (222) => (221) => (211) => (111). The modulation sequence contains redundant states for V_1, V_2, and V_7. From the perspective of space vector modulation, it can be observed that this sequence corresponds to the D_7 sector in the space vector diagram (see Fig. 3). A comparison in Fig. 11 reveals that the amplitude of the output voltage modulated by the COPWM method is larger than that of the conventional SVPWM method.

As stated in [29] and [30], under the same modulation index, the amplitude of the output voltage is the same for both SVPWM and CBPWM methods. Therefore, when comparing the relationship between the output voltage amplitudes of the SVPWM and COPWM methods, it is reasonable to use the output voltage amplitude of the CBPWM method as a representation of the output voltage amplitude of the SVPWM method. The schematic diagram of the output voltage U_{AO} for the CBPWM method and

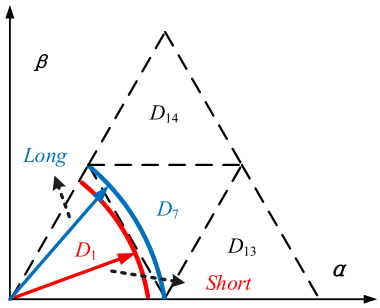

Fig. 11. Comparison of reference vector in Sector D_1 and Sector D_7.

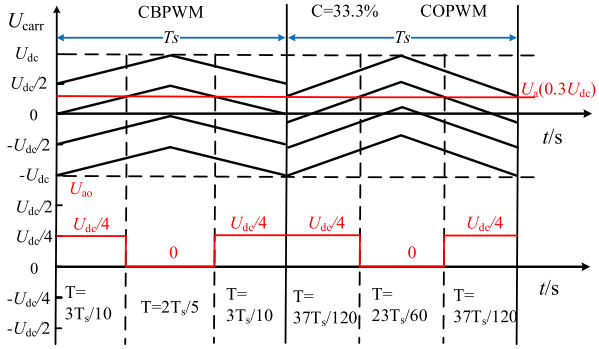

Fig. 12. Schematic diagram of COPWM($C = 33.3\%$) and CBPWM method U_{AO} when $m = 0.3$.

the COPWM($C = 33.3\%$) method when $m = 0.3$ is shown in Fig. 12.

As shown in Fig. 11, the amplitude of the output voltage U_{AO} throughout one switching cycle can be obtained through the area averaging method, as demonstrated in

$$\begin{cases} \text{CBPWM}: 2 \times \frac{3T_s}{10} \times \frac{U_{dc}}{4} + 0 = 0.3 \times \frac{U_{dc} \times T_s}{2} \\ \text{COPWM}: 2 \times \frac{37T_s}{120} \times \frac{U_{dc}}{4} + 0 = \frac{37}{120} \times \frac{U_{dc} \times T_s}{2} \end{cases}. \tag{4}$$

Since $0.3 < 37/120$, it is evident that the amplitude of the output voltage is greater in the COPWM($C = 33.3\%$) method compared to the CBPWM method, which means it is also greater than the SVPWM method. Analyzing the impact of varying overlap ratios on the amplification effect of the output voltage, it is advisable to employ a similar approach to analyze the COPWM ($C = 83.3\%$) method, and subsequently compare it with the COPWM ($C = 33.3\%$) method.

The schematic diagram of the output voltage U_{AO} for the CBPWM method and the COPWM ($C = 83.3\%$) method at $m = 0.3$ is shown in Fig. 13.

By comparing the output voltages of the CBPWM and COPWM methods in Fig. 13, the magnitude of the output voltage U_{AO} within one switching cycle can be obtained using the area average method

$$\begin{cases} \text{CBPWM}: \\ 2 \times \frac{3T_s}{10} \times \frac{U_{dc}}{4} + 0 = 0.3 \times \frac{U_{dc} \times T_s}{2} \\ \text{COPWM}: \\ \frac{19T_s}{40} \times \frac{U_{dc}}{2} + \frac{T_s}{6} \times \frac{U_{dc}}{4} \\ -\left(\frac{T_s}{6} \times \frac{U_{dc}}{4} + \frac{T_s}{40} \times \frac{U_{dc}}{2}\right) = \frac{9}{20} \times \frac{U_{dc} \times T_s}{2} \end{cases}. \tag{5}$$

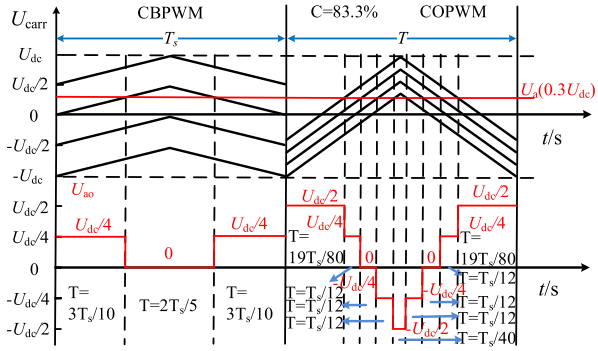

Fig. 13. Schematic diagram of COPWM($C = 83.3\%$) and CBPWM method U_{AO} at $m = 0.3$.

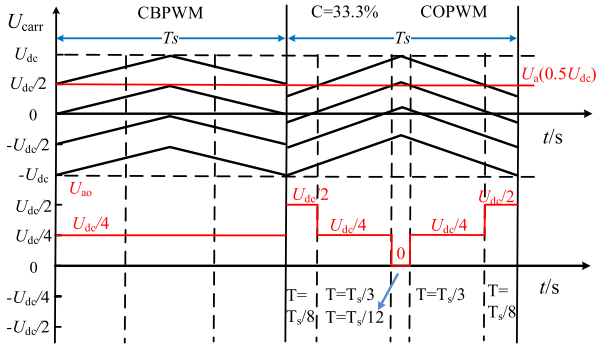

Fig. 14. Schematic diagram of COPWM($C = 33.3\%$) and CBPWM method U_{AO} when $m = 0.5$.

Since $0.3 < 37/120 < 9/20$, it is easy to deduce that the magnitude of the output voltage under the COPWM($C = 83.3\%$) method is larger than that under the CBPWM method. Consequently, it can be inferred that the output voltage magnitude under the COPWM($C = 83.3\%$) method is greater than that under the SVPWM method at the same modulation index. By comparing (4) and (5), it can be observed that as the overlap ratio increases, the amplification of the output voltage also increases. However, upon closer examination of the amplification magnitude, it becomes evident that the effect of the overlap ratio on the amplification of the output voltage magnitude is not linear. The overlap ratio ranged from 33.3% to 83.3%. However, the amplification magnitude of the output voltage changed from 1.028 to 1.5.

The schematic diagram of the output voltage U_{AO} for the CBPWM method and the COPWM($C = 33.3\%$) method when $m = 0.5$ and $m = 0.8$ is shown in Figs. 14 and 15.

From Fig. 14, it can be seen that the CBPWM peak output voltage expression and the COPWM peak output voltage expression are as follows when the modulation index $m = 0.5$:

$$\begin{cases} \text{CBPWM}: T_s \times \frac{U_{dc}}{4} = 0.5 \times \frac{U_{dc} \times T_s}{2} \\ \text{COPWM}: \frac{T_s}{4} \times \frac{U_{dc}}{2} + \frac{2T_s}{3} \times \frac{U_{dc}}{4} = \frac{7}{12} \times \frac{U_{dc} \times T_s}{2} \end{cases}. \tag{6}$$

At this juncture, the peak output voltage of COPWM surpasses that of CBPWM by 116.67%. The expressions for the peak output voltages in CBPWM and COPWM at a modulation

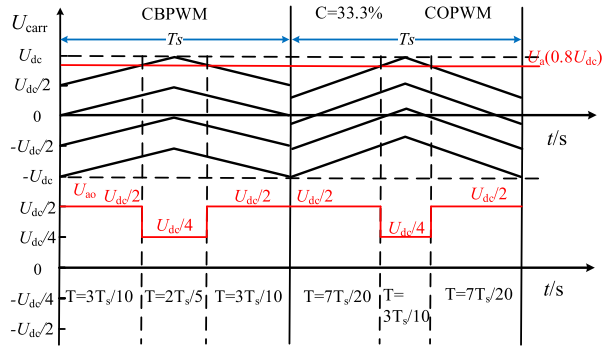

Fig. 15. Schematic diagram of COPWM($C = 33.3\%$) and CBPWM method U_{AO} when $m = 0.8$.

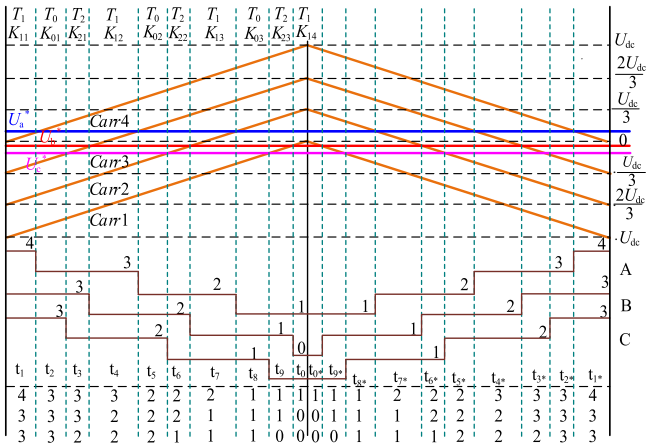

Fig. 16. Equivalent schematic diagram of COPWM method and SVPWM method.

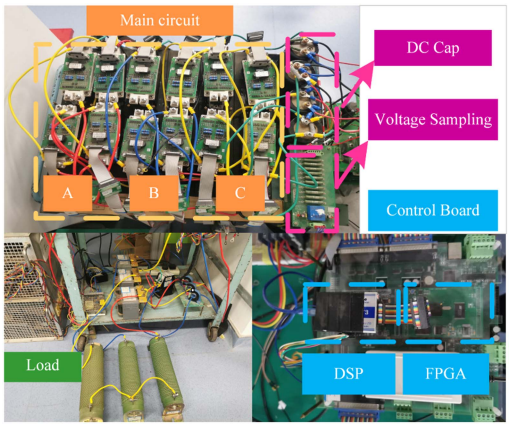

Fig. 17. NPC five-level experimental platform.

index of $m = 0.8$ are provided as follows:

$$\begin{cases} \text{CBPWM}: \frac{3T_s}{5} \times \frac{U_{dc}}{2} + \frac{2T_s}{5} \times \frac{U_{dc}}{4} = 0.8 \times \frac{U_{dc} \times T_s}{2} \\ \text{COPWM}: \frac{7T_s}{10} \times \frac{U_{dc}}{2} + \frac{3T_s}{10} \times \frac{U_{dc}}{4} = \frac{17}{20} \times \frac{U_{dc} \times T_s}{2} \end{cases}. \quad (7)$$

At this juncture, the peak output voltage of COPWM surpasses that of CBPWM by 106.25%. When the overlap ratio remains constant, the amplification of the COPWM method's

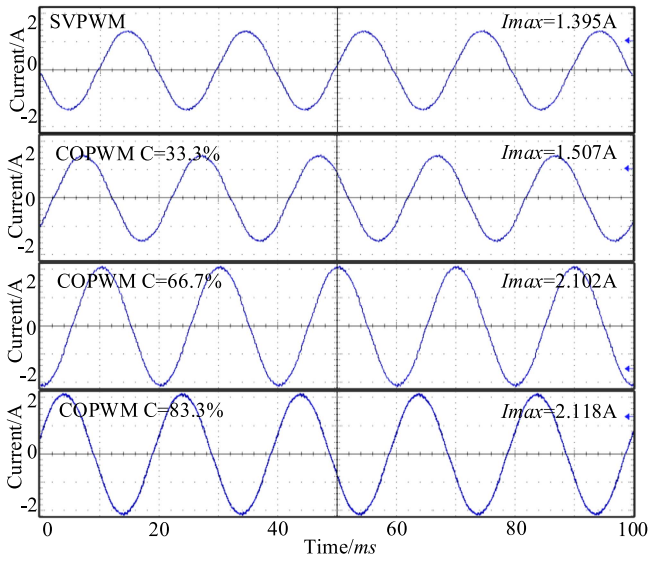

Fig. 18. Output phase-A current waveforms under four modulation methods, when $m = 0.3$.

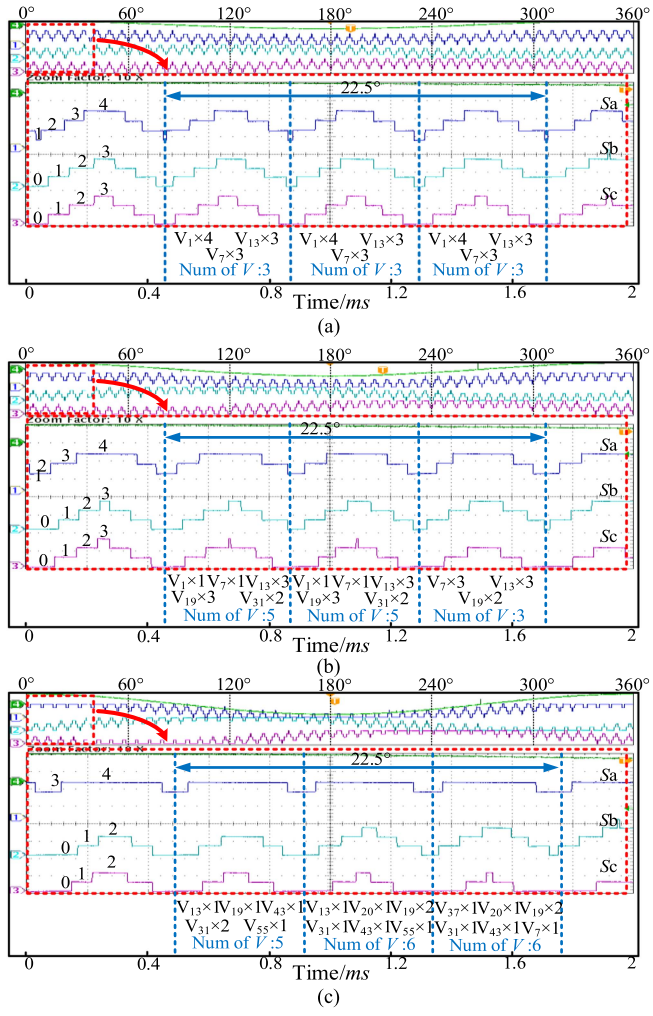

Fig. 19. Voltage level states of the three-phase outputs A, B, and C in the COPWM ($C = 66.7\%$) method. (a) $m = 0.3$. (b) $m = 0.5$. (c) $m = 0.8$.

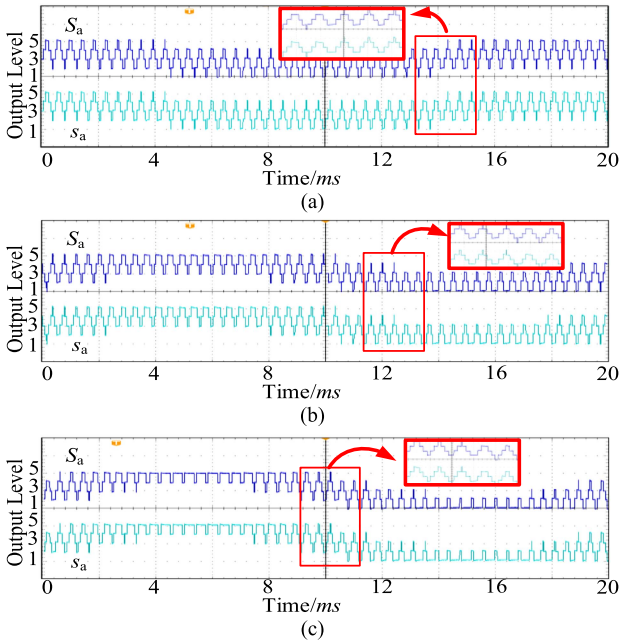

Fig. 20. Output level states under two modulation methods. (a) $m = 0.3$. (b) $m = 0.5$. (c) $m = 0.8$.

peak output voltage decreases as the modulation increases. Notably, when modulation index reaches a value of 1, there is no amplification effect observed. This characteristic must be considered during the equivalence analysis.

B. Equivalent Analysis of COPWM Method to SVPWM Method

After analyzing the modulation sequence using a similar analysis method as in Section IV-A, it is possible to achieve the same modulation effect as the COPWM method using the SVPWM method. This article introduces the method using $C = 66.7\%$ and $m = 0.1$ as an example. Fig. 16 illustrates the schematic diagram of the modulation sequence generated by the COPWM method when the modulation index is 0.1. From the figure, it can be observed that the modulation sequence for one switching period is as follows: (433) $=>$ (333) $=>$ (332) $=>$ (322) $=>$ (222) $=>$ (221) $=>$ (211) $=>$ (111) $=>$ (110) $=>$ (100). The switching states (433), (322), (211), and (100) correspond to the four redundant switching states of V_1 in the SVPWM space vector diagram, while (333), (222), and (111) correspond to the three redundant switching states of V_0 in the space vector diagram, and (332), (221), (110) correspond to the three redundant switching states of V_2 in the space vector diagram.

By arranging the occurrence order of the redundant states of vectors V_1, V_0, and V_2 reasonably and assigning equal operating time to each redundant state as obtained by the COPWM method, it is possible to achieve the same modulation effect using the SVPWM method.

Next, the calculation method for the operating time of each equivalent SVPWM vector and the proportion of redundant states will be provided.

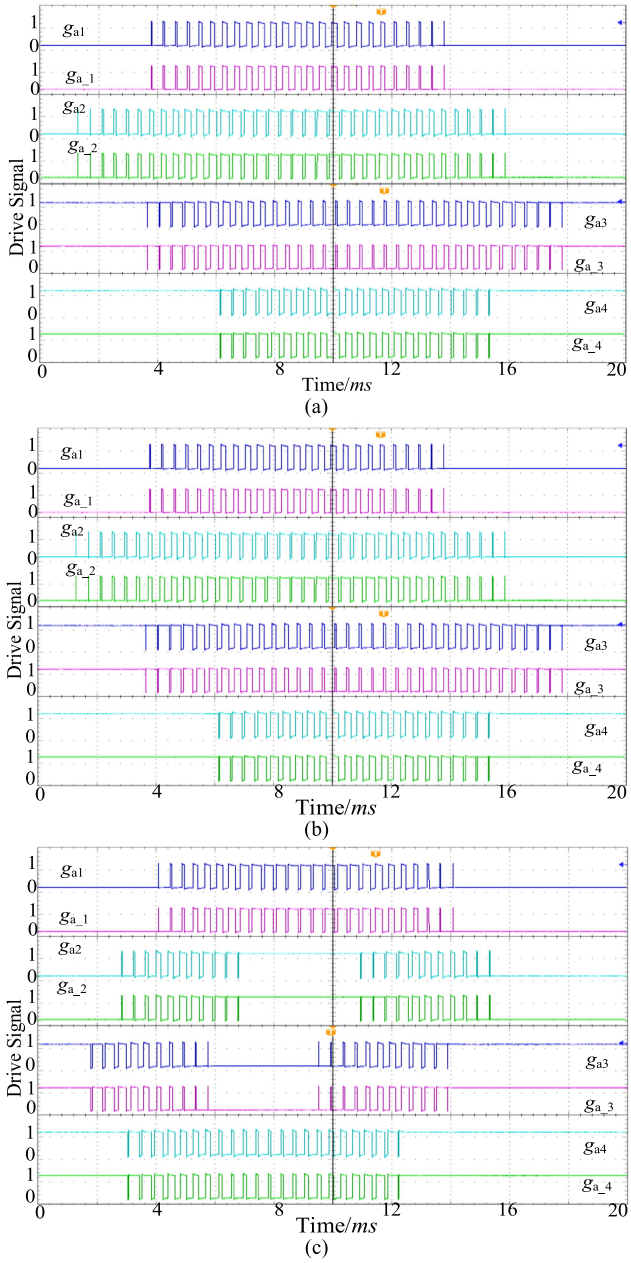

Fig. 21. Drive signal of the four switches of phase A under two modulation methods. (a) $m = 0.3$. (b) $m = 0.5$. (c) $m = 0.8$.

Within one switching period, as shown in Fig. 16, the time intervals $t_0 \sim t_9$ and $t_{0*} \sim t_{9*}$ can be obtained using the principle of similar triangles, as shown in

$$\begin{cases} t_1 = t_{1*} = \frac{U_a \times T_s}{2U_{\rm dc}}, t_2 = t_{2*} = \frac{(U_{\rm dc}/3 + U_{ca}) \times T_s}{2U_{\rm dc}} \\ t_3 = t_{3*} = \frac{U_{bc} \times T_s}{2U_{\rm dc}}, t_4 = t_{4*} = \frac{U_{ab} \times T_s}{2U_{\rm dc}} \\ t_5 = t_{5*} = \frac{(U_{\rm dc}/3 + U_{ca}) \times T_s}{2U_{\rm dc}}, t_6 = t_{6*} = \frac{U_{\rm bc} \times T_s}{2U_{\rm dc}} \\ t_7 = t_{7*} = \frac{U_{ab} \times T_s}{2U_{\rm dc}}, t_8 = t_{8*} = \frac{(U_{\rm dc}/3 + U_{ca}) \times T_s}{2U_{\rm dc}} \\ t_9 = t_{9*} = \frac{U_{bc} \times T_s}{2U_{\rm dc}}, t_0 = t_{0*} = -\frac{U_b \times T_s}{2U_{\rm dc}} \end{cases} . \quad (8)$$

The working time of each redundant state for each vector can be summed up to obtain the duty cycle of that vector within one switching period. In the equation, t_1, t_4, t_7, t_0, t_{1*}, t_{4*}, t_{7*}, and t_{0*} represent the working time for vector V_1, t_2, t_5, t_8, t_{2*}, t_{5*}, and t_{8*} represent the working time for vector V_0, and t_3, t_6, t_9, t_{3*}, t_{6*}, and t_{9*} represent the working time for vector V_2. Therefore, the working times T_0, T_1, and T_2 for vectors V_0, V_1, and V_2 can be obtained as follows:

$$\begin{cases} T_1 = t_1 + t_{1*} + t_4 + t_{4*} + t_7 + t_{7*} + t_0 + t_{0*} \\ = 2 \times (2 \times \frac{U_{ab} \times T_s}{2U_{\mathrm{dc}}} + \frac{U_a \times T_s}{2U_{\mathrm{dc}}} - \frac{U_b \times T_s}{2U_{\mathrm{dc}}}) = \frac{3U_{ab} \times T_s}{U_{\mathrm{dc}}} \\ T_0 = t_2 + t_{2*} + t_5 + t_{5*} + t_8 + t_{8*} \\ = 2 \times 3 \times \frac{(U_{\mathrm{dc}}/3 + U_{ca}) \times T_s}{2U_{\mathrm{dc}}} = \frac{(U_{\mathrm{dc}} + 3U_{ca}) \times T_s}{U_{\mathrm{dc}}} \\ T_2 = t_3 + t_{3*} + t_6 + t_{6*} + t_9 + t_{9*} \\ = 2 \times 3 \times \frac{U_{bc} \times T_s}{2U_{\mathrm{dc}}} = \frac{3U_{bc} \times T_s}{U_{\mathrm{dc}}} \end{cases} . \quad (9)$$

In the conventional SVPWM modulation method, after obtaining the working time of each vector within one switching period, it is customary to use time allocation coefficients to represent the proportion of each redundant state's working time to the total working time of the vector. The working time of each vector's redundant state is then expressed by multiplying the time allocation coefficient by the total working time of the vector. Let K_{01}, K_{02}, and K_{03} represent the time allocation coefficients for the redundant states of vector V_0. Similarly, K_{11}, K_{12}, K_{13}, and K_{14} represent the time allocation coefficients for the redundant states of vector V_1, while K_{21}, K_{22}, and K_{23} represent the time allocation coefficients for the redundant states of vector V_2. By combining (8) and (9), the expression for the time allocation coefficients can be derived as shown in

$$\begin{cases} K_{01} = K_{02} = K_{03} = \frac{1}{3} \\ K_{11} = \frac{U_a}{3U_{ab}}, K_{12} = K_{13} = \frac{1}{3}, K_{14} = \frac{-U_b}{3U_{ab}} \\ K_{21} = K_{22} = K_{23} = \frac{1}{3} \end{cases} . \quad (10)$$

By combining the switching sequence in Fig. 13, the working time of vectors V_0, V_1, and V_2 as mentioned in (9), and the time allocation coefficients for each redundant state as expressed in (10), the correct working time and arrangement of each vector's redundant state can be achieved within one cycle. By doing so, it effectively replicates the output effect of the COPWM method using the SVPWM method.

V. Experimental Verification

To validate the accuracy of the proposed content in this article, an experimental platform was established based on a digital signal processor (DSP)/field programmable gate array (FPGA) hardware platform. The experimental setup involved a five-level NPC inverter with the main circuit topology depicted in Fig. 1. The control board comprised a DSP (TMS320F28346) from TI and an FPGA (XC6SLX25) from Xilinx. Since modulation is an open-loop system, the equivalence relationship can be verified by observing the PWM output pulses of the controller. The experimental parameters are given in Table II.

The construction of the experimental setup for the five-level NPC inverter is illustrated in Fig. 17.

TABLE II
Experiment Parameters

Parameters	Value
DC Voltage Vdc	100V
Switching Frequency fs	2.4kHz
Load R	10Ω
Leg Inductance L1	7mH
Overlap ratio(C)	66.7%

The waveform shown in Fig. 16 represents the experimental results of the phase A output current in the five-level NPC inverter for $m = 0.3$ using the SVPWM method, COPWM ($C = 33.3\%$) method, COPWM ($C = 66.7\%$) method, and COPWM ($C = 83.3\%$) method. It can be observed from Fig. 18 that, as the carrier overlapping ratio deepens, the amplitude of the output current increases under the same modulation index. By comparing the output current between $C = 66.7\%$ and $C = 33.3\%$, as well as between $C = 83.3\%$ and $C = 66.7\%$, it is evident that the amplification effect of the output current is not linear.

Fig. 19(a), (b), and (c) depicted the voltage level states of phases A, B, and C, respectively, under the COPWM ($C = 66.7\%$) method for $m = 0.1$, 0.3, and 0.5.

From Fig. 19(a), it can be observed that when $m = 0.3$ and the reference vector is located in the sector I, three vectors are used for the synthesis of the reference vector within one switching period. Fig. 19(b) indicates that when $m = 0.5$ and the reference vector is between 0° and 15° in the sector I, five vectors are used for the synthesis of the reference vector within one switching period, while from 15° to 30°, three vectors are used. Fig. 19(c) reveals that when $m = 0.8$ and the reference vector is between 0° and 7.5° in the sector I, five vectors around the reference vector are used for vector synthesis. From 7.5° to 30°, six vectors around the reference vector are used for the synthesis of the reference vector. Hence, it can be inferred that as the modulation index increases, the equivalent reference vector synthesis method of the COPWM ($C = 66.7\%$) method transitions from the conventional SVPWM's closest three-vector synthesis to the synthesis of multiple vectors around the reference vector, which is different from the conventional SVPWM method.

Fig. 20(a), (b), and (c) illustrates the voltage level states of phase A output, s_a and S_a, for modulation indices $m = 0.3$, 0.5, and 0.8. Here, s_a represents the output voltage level state of phase A in the COPWM method, while S_a represents the output voltage level state of phase A in the SVPWM method. From the figures, it can be observed that the voltage level state of phase A in the equivalent SVPWM method proposed in this article is identical to that of the COPWM method. This is because the overlap ratio C is set at 66.7%, ensuring that there is no overlap between carrier 1 and carrier 4. Consequently, it can be deduced that a maximum of four distinct voltage levels will occur within a single switching period.

Fig. 21(a), (b), and (c) depict the comparison between the driving signals, $g_{a1}(g_{a\_1})$, $g_{a2}(g_{a\_2})$, $g_{a3}(g_{a\_3})$, and $g_{a4}(g_{a\_4})$, generated by the two modulation methods for switches S_{a1}, S_{a2}, S_{a3}, and S_{a4} in Fig. 1, corresponding to

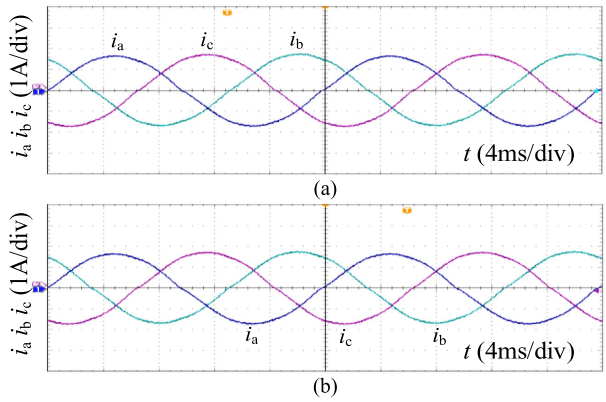

Fig. 22. Output three-phase current waveforms under two modulation methods, when $m = 0.3$. (a) Carrier overlapping pulsewidth modulation. (b) Equivalent SVPWM.

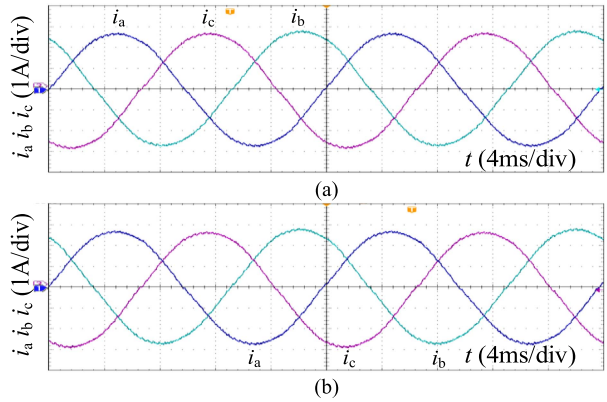

Fig. 23. Output three-phase current waveforms under two modulation methods, when $m = 0.5$. (a) Carrier overlapping pulsewidth modulation. (b) Equivalent SVPWM.

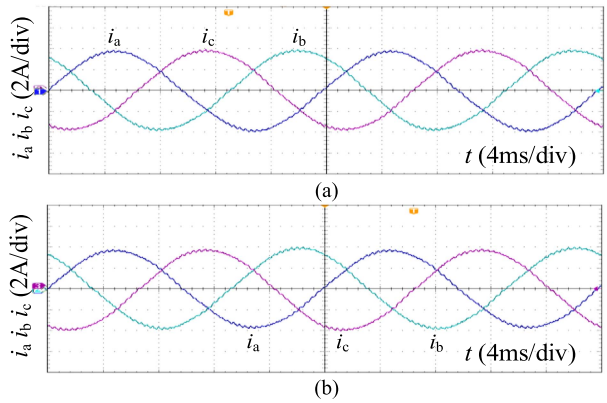

Fig. 24. Output three-phase current waveforms under two modulation methods, when $m = 0.8$. (a) Carrier overlapping pulsewidth modulation. (b) Equivalent SVPWM.

modulation indices $m = 0.3$, 0.5, and 0.8. The switch states $g_{ai}(i = 1\text{-}4)$ are generated using the COPWM method, while $g_{a\_i}(i = 1\text{-}4)$ are generated using the equivalent SVPWM method proposed in this article.

By comparing the waveforms, it can be observed that the switch states $g_{ai}(i = 1\text{-}4)$ are identical to the switch states, $g_{a\_i}(i = 1\text{-}4)$. Combining this observation with Fig. 21, it can be concluded that both methods yield identical output pulses and exhibit the same output characteristics. This validates the effectiveness of the proposed equivalent method. Figs. 22, 23, and 24 illustrate the three-phase current waveforms produced by both modulation techniques for modulation indices $m = 0.3$, 0.5, and 0.8. The three-phase current waveforms generated by both modulation methods are consistent. In conclusion, the equivalent strategy proposed in this article is accurate and effective.

VI. Conclusion

This article investigates the fundamental principles of the COPWM method and SVPWM method for a five-level diode-clamped inverter. Through the investigation, it is revealed that the synthesis method of the equivalent reference vector in the COPWM method is influenced by two variables: modulation index and overlap ratio. As the modulation index increases and the overlap ratio deepens, the equivalent spatial vector partition changes from the nearest three-vector synthesis reference vector, similar to conventional SVPWM, to multiple vectors surrounding the reference vector, distinct from conventional SVPWM.

Furthermore, when both COPWM and SVPWM strategies employ the same modulation index, the line voltage amplitude produced by the COPWM method is amplified. However, this amplification is not linear and depends on the overlap ratio and modulation index.

Finally, the article proposes an implementation approach for achieving the equivalent effects of the COPWM method using the SVPWM method. Experimental validation confirms the correctness and effectiveness of this approach.

References

[1] Z. Gao, Q. Ge, Y. Li, L. Zhao, B. Zhang, and K. Wang, "Hybrid improved carrier-based PWM strategy for three-level neutral-point-clamped inverter with wide frequency range," *IEEE Trans. Power Electron.*, vol. 36, no. 7, pp. 8517–8538, Jul. 2021.

[2] S. K. Giri, S. Chakrabarti, S. Banerjee, and C. Chakraborty, "A carrier-based PWM scheme for neutral point voltage balancing in three-level inverter extending to full power factor range," *IEEE Trans. Ind. Electron.*, vol. 64, no. 3, pp. 1873–1883, Mar. 2017.

[3] S. K. Giri, S. Mukherjee, S. Kundu, S. Banerjee, and C. Chakraborty, "An improved PWM scheme for three-level inverter extending operation into overmodulation region with neutral-point voltage balancing for full power-factor range," *IEEE J. Emerg. Sel. Topics Power Electron.*, vol. 6, no. 3, pp. 1527–1539, Sep. 2018.

[4] W. Song, X. Feng, and K. M. Smedley, "A carrier-based PWM strategy with the offset voltage injection for single-phase three-level neutral-point-clamped converters," *IEEE Trans. Power Electron.*, vol. 28, no. 3, pp. 1083–1095, Mar. 2013.

[5] J. Wang, Y. Gao, and W. Jiang, "A carrier-based implementation of virtual space vector modulation for neutral-point-clamped three-level inverter," *IEEE Trans. Ind. Electron.*, vol. 64, no. 12, pp. 9580–9586, Dec. 2017.

[6] H. Zheng, B. Zhu, H. Zhang, and L. Chen, "Carrier overlaping-switch frequency optional PWM method for cascaded multilevel inverter," in *Proc. Int. Conf. Elect. Control Eng.*, 2010, pp. 3450–3453.

[7] H. Wang, Y. Deng, and X. He, "Novel carrier-based PWM method with voltage balance for flying capacitor multilevel inverters," in *Proc. IEEE 35th Annu. Power Electron. Specialists Conf.*, 2004, pp. 4423–4427 vol. 6.

[8] K. Wang, Z. Zheng, and Y. Li, "A novel carrier-overlapped PWM method for four-level neutral-point clamped converters," *IEEE Trans. Power Electron.*, vol. 34, no. 1, pp. 7–12, Jan. 2019.

[9] K. Wang, Z. Zheng, L. Xu, and Y. Li, "A generalized carrier-overlapped PWM method for neutral-point-clamped multilevel converters," *IEEE Trans. Power Electron.*, vol. 35, no. 9, pp. 9095–9106, Sep. 2020.
[10] K. Wang, Z. Zheng, L. Xu, and Y. Li, "Neutral-point voltage balancing method for five-level NPC inverters based on carrier-overlapped PWM," *IEEE Trans. Power Electron.*, vol. 36, no. 2, pp. 1428–1440, Feb. 2021.
[11] K. Wang, Z. Zheng, L. Xu, and Y. Li, "A composite voltage-balancing method for four-level NPC inverters," *IEEE J. Emerg. Sel. Topics Power Electron.*, vol. 9, no. 3, pp. 3394–3406, Jun. 2021.
[12] K. Wang, Z. Zheng, and Y. Li, "Topology and control of a four-level ANPC inverter," *IEEE Trans. Power Electron.*, vol. 35, no. 3, pp. 2342–2352, Mar. 2020.
[13] S. Wang, J. Ma, B. Liu, N. Jiao, T. Liu, and Y. Wang, "Unified SVPWM algorithm and optimization for single-phase three-level NPC converters," *IEEE Trans. Power Electron.*, vol. 35, no. 7, pp. 7702–7712, Jul. 2020.
[14] A. K. Gupta and A. M. Khambadkone, "A space vector PWM scheme for multilevel inverters based on two-level space vector PWM," *IEEE Trans. Ind. Electron.*, vol. 53, no. 5, pp. 1631–1639, Oct. 2006.
[15] A. R. Beig, G. Narayanan, and V. T. Ranganathan, "Modified SVPWM algorithm for three level VSI with synchronized and symmetrical waveforms," *IEEE Trans. Ind. Electron.*, vol. 54, no. 1, pp. 486–494, Feb. 2007.
[16] Y. Deng, Y. Wang, K. H. Teo, and R. G. Harley, "A simplified space vector modulation scheme for multilevel converters," *IEEE Trans. Power Electron.*, vol. 31, no. 3, pp. 1873–1886, Mar. 2016.
[17] C. Wang et al., "SVPWM strategy based on the 45°coordinates to suppress common-mode voltage for multilevel converters," *IEEE Trans. Power Electron.*, vol. 38, no. 2, pp. 1984–1997, Feb. 2023.
[18] N. Celanovic and D. Boroyevich, "A comprehensive study of neutral-point voltage balancing problem in three-level neutral-point-clamped voltage source PWM inverters," *IEEE Trans. Power Electron.*, vol. 15, no. 2, pp. 242–249, Mar. 2000.
[19] S. Das and G. Narayanan, "Novel switching sequences for a space-vector-modulated three-level inverter," *IEEE Trans. Ind. Electron.*, vol. 59, no. 3, pp. 1477–1487, Mar. 2012.
[20] X. Peng, X. He, P. Han, H. Lin, S. Gao, and Z. Shu, "Opposite vector based phase shift carrier space vector pulse width modulation for extending the voltage balance region in single-phase 3LNPC cascaded rectifier," *IEEE Trans. Power Electron.*, vol. 32, no. 9, pp. 7381–7393, Sep. 2017.
[21] Z. Li, Y. Guo, J. Xia, Y. Duan, and X. Zhang, "Modified synchronized SVPWM strategies to reduce CMV for three-phase VSIS at low switching frequency," *IEEE Trans. Ind. Appl.*, vol. 56, no. 5, pp. 5245–5256, Sep./Oct. 2020.
[22] B. Yu, W. Song, and Y. Guo, "A simplified and generalized SVPWM scheme for two-level multiphase inverters with common-mode voltage reduction," *IEEE Trans. Ind. Electron.*, vol. 69, no. 2, pp. 1378–1388, Feb. 2022.
[23] H. Xu, W. Yao, and S. Shao, "Improved SVPWM schemes for vienna rectifiers without current distortion," in *Proc. IEEE Energy Convers. Congr. Expo.*, 2017, pp. 3410–3414.
[24] Q. Yan et al., "Optimization of the symmetrical SVPWM for three-level T-type inverters with unbalanced and oscillated neutral-point voltages," *IEEE Trans. Ind. Electron.*, vol. 71, no. 4, pp. 4026–4037, Apr. 2024.
[25] Q. Yan, Z. Zhou, M. Wu, X. Yuan, R. Zhao, and H. Xu, "A simplified analytical algorithm in abc coordinate for the three-level SVPWM," *IEEE Trans. Power Electron.*, vol. 36, no. 4, pp. 3622–3627, Apr. 2021.
[26] R. Cheng, Y. He, C. Lei, Y. Wang, and J. Liu, "Research on realizing space vector equivalent modulation output by dual carrier modulation of current source inverter," *IEEE Trans. Power Electron.*, vol. 36, no. 7, pp. 8494–8505, Jul. 2021.
[27] J. Chen, Y. He, S. U. Hasan, and J. Liu, "A Comprehensive study on equivalent modulation waveforms of the SVM sequence for three-level inverters," *IEEE Trans. Power Electron.*, vol. 30, no. 12, pp. 7149–7158, Dec. 2015.
[28] Y. He, Y. Liu, C. Lei, and J. Liu, "Equivalent space vector output of diode clamped multilevel inverters through modulation wave decomposition under carrier-based PWM Strategy," *IEEE Access*, vol. 8, pp. 104918–104932, 2020.
[29] K. Zhou and D. Wang, "Relationship between space-vector modulation and three-phase carrier-based PWM: A comprehensive analysis [three-phase inverters]," *IEEE Trans. Ind. Electron.*, vol. 49, no. 1, pp. 186–196, Feb. 2002.
[30] R. Burgos, R. Lai, Y. Pei, F. Wang, D. Boroyevich, and J. Pou, "Space vector modulation for Vienna-type rectifiers based on the equivalence between two- and three-level converters: A carrier-based implementation," *IEEE Trans. Power Electron.*, vol. 23, no. 4, pp. 1888–1898, Jul. 2008.

Haoting Du (Student Member, IEEE) received the B.S. degree in electrical engineering from the China Agricultural University, Beijing, China, in 2021. He is currently working torward the Ph.D. degree in electrical engineering with Xi'an Jiaotong University, Xi'an, in China.

His research interest is modulation strategy of multilevel Inverters.

Yingjie He (Senior Member, IEEE) received the B.S. degree in mechanical engineering from Huazhong Universityof Science and Technology, Wuhan, China, in 1999, the M.S. and Ph.D. degrees in electrical engineering from Huazhong Universityof Science and Technology, Wuhan, China, in 2003, and 2007, respectively.

He was with the Power Electronics and Renewable Energy Center, Xi'an Jiaotong University (XJTU), Xi'an, China, as a Postdoctoral Researcher, and with Aalborg University, Aalborg, Denmark, as a Visiting Scholar. He is currently an Associate Professor and a Doctoral Supervisor with XJTU. He is selected as the High-level Talent of Shaanxi Power Supply Society and the High-level Talent of Zhenjiang, Jiangsu. He is the Executive Director of IEEE Flexible AC Transmission Technology Subcommittee (China), the Executive Director of Shaanxi Power Supply Society, Senior Member of China Electrotechnical Society, a Member of Power Quality Special Committee of China Power Supply Society, and an Appraisal Expert of National Natural Science Foundation and Ministry of Science and Technology of China. He has published over 100 journal and conference papers, such as IEEE TRANSACTIONS ON POWER ELECTRONICS and IEEE TRANSACTIONS ON INDUSTRIAL ELECTRONICS. His research interests include multilevel converter and its control technology, application of power electronics in power system, power quality and its control technology.

Dr. He was the recipient of the Second Prize of Science and Technology Progress from China Power Supply Society in 2021, the Science and Technology Progress Award from Shaanxi Power Supply Society in 2022, and the Special Contribution Award from Proceedings of the CSEE.

Zhengchen Zhao received the B.S. degree in electrical engineering from the Xinjiang University, Urumqi, China, in 2022. He is currently working torward the M.S. degree in electrical engineering with Xi'an Jiaotong University, Xi'an, China.

His research interest is modulation strategy of multilevel Inverters.

Shenglun Zhuang received the Ph.D degree in power electronics and power drives from Nanjing University of Aeronautics and Astronautics, Nanjing, China, in 2017.

He is currently an Engineer with Nari Group Corporation, Nanjing, China. His research interests include new energy generation and high-power electronic devices.

Jinjun Liu (Fellow, IEEE) received the B.S. and Ph.D. degrees in electrical engineering from Xi'an Jiaotong University (XJTU), Xi'an, China, in 1992 and 1997, respectively.

He was a Faculty of the XJTU Electrical Engineering School. From late 1999 to early 2002, he was with the Center for Power Electronics Systems, Virginia Polytechnic Institute and State University, Blacksburg, VA, USA, as a Visiting Scholar. In late 2002, he was a Full Professor and then the Head of the Power Electronics and Renewable Energy Center with XJTU, which now comprises 21 faculty members and more than 150 graduate students and carries one of the leading power electronics programs in China. From 2005 to early 2010, he was an Associate Dean of Electrical Engineering School at XJTU, and from 2009 to early 2015, the Dean for Undergraduate Education of XJTU. He is currently a XJTU Distinguished Professor of Power Electronics. He coauthored 3 books (including one textbook), authored or coauthored more 400 technical papers in peer-reviewed journals and conference proceedings, holds more than 50 invention patents (China/US/Europe), and delivered for many times plenary keynote speeches and tutorials at IEEE conferences or China national conferences in power electronics area. His research interests include modeling, control, and design methods for power converters and electronified power systems, power quality control and utility applications of power electronics, and micro-grids for sustainable energy and distributed generation.

Dr. Liu was the recipient of for eight times governmental awards at national level or provincial/ministerial level for scientific research/teaching achievements. He is also the recipeint of 2006 Delta Scholar Award, the 2014 Chang Jiang Scholar Award, the 2014 Outstanding Sci-Tech Worker of the Nation Award, the 2016 State Council Special Subsidy Award, and the IEEE Transactions on Power Electronics 2016 Prize Paper Award. He was the IEEE Power Electronics Society Region 10 Liaison and then China Liaison for ten years, an Associate Editor for IEEE TRANSACTIONS ON POWER ELECTRONICS for 13 years, 2015–2019 Executive Vice President and 2020–2021 Vice President for membership of IEEE PELS. He is on the Board of China Electrotechnical Society and was elected the Vice President in 2013 and the Secretary General in 2018 of the CES Power Electronics Society. Since 2013, he has been the Vice President for International Affairs, China Power Supply Society and since 2016, the inaugural Editor-in-Chief for *CPSS Transactions on Power Electronics and Applications*. Since 2013, he has been the Vice Chair of the Chinese National Steering Committee for College Electric Power Engineering Programs.